Journal of Geochemical Exploration 190 (2018) 424–435

Contents lists available at ScienceDirect

Journal of Geochemical Exploration

journal homepage: www.elsevier.com/locate/gexplo

Uranium enrichment in a paleo-karstic bauxite deposit, Yunfeng, SW China: Mineralogy, geochemistry, transport – deposition mechanisms and significance for uranium exploration

Yongzhen Long[a,b], Guoxiang Chi[c,*], Jianping Liu[a,b], Dexian Zhang[a,b], Hao Song[c,d]

[a] Key Laboratory of Metallogenic Prediction of Nonferrous Metals and Geological Environment Monitoring, Ministry of Education, Central South University, Changsha 410083, China
[b] School of Geosciences and Info-Physics, Central South University, Changsha 410083, China
[c] Department of Geology, University of Regina, Saskatchewan, S4S 0A2, Canada
[d] Chengdu University of Technology, Chengdu, 610059, China

ARTICLE INFO

Keywords:
Paleo-karstic
Bauxite deposit
Uranium minerals
EPMA
Raman spectroscopy
Yunfeng
Guizhou

ABSTRACT

Elevated concentrations of uranium have been found in many bauxite deposits, but the status of uranium in the ores and the mechanisms of enrichment have not been well understood. In this paper, we report a new case of uranium enrichment in a paleo-karstic bauxite deposit at Yunfeng, southwestern China, present electron probe micro-analyzer (EPMA) and Raman spectroscopic evidence for the presence of separate U-minerals, and propose a model in which uranium was enriched through successive processes from chemical weathering through early to burial diagenesis. The Yunfeng bauxite ores, developed in Lower Carboniferous mudrocks overlying Middle to Upper Cambrian carbonate rocks, contain 18.0 to 62.4 ppm (average 35.1 ppm) U, which is much high than the abundances in average crustal rocks (1–3 ppm). Micron-sized uraninite occurs as rims of Ti-oxides, fillings of micro-fractures in kaolinite, and disseminated grains in association with sulfides in the matrix of diaspore and kaolinite. Trace and rare earth elements analysis indicates that the bauxite ores could not be produced by in-situ weathering of the carbonates underlying the orebodies. Instead, the precursor rocks of the bauxite ores are inferred to be black shales originally enriched in uranium that were exposed tens of kilometers away. Detrital grains of the black shales were transported and accumulated in depressions above karstified carbonates in the Yunfeng area, where they were subjected to intense weathering to form bauxite ores. The weathering of the shale clasts liberated much of the uranium due to oxidation of uranium from U^{4+} to U^{6+}. However, the majority of the U^{6+} was reduced to U^{4+} again due to availability of reducing agents such as organic matter and sulfides originally in the shales, forming nanocrystals of UO_{2+x} in close association with Ti-oxides disseminated in Al-hydroxides and clay minerals. These nanocrystals of UO_{2+x} were converted to uraninite during diagenesis, together with the convention of gibbsite and boehmite to diaspore and the formation of anhedral to euhedral pyrite and various Cu-, Pb-, Ni- and Co-rich sulfides. The recognition of uraninite in the bauxite ores is important for uranium exploration and for evaluation of the economic value of uranium as a byproduct of bauxite deposits.

1. Introduction

Many studies have revealed that bauxite ores may contain elevated concentrations of uranium that are significantly above the average crustal abundances (approximately 1 to 3 ppm, see Cumberland et al., 2016), for example, up to 26.7 ppm (average 11.4 ppm) in 29 bauxite deposits worldwide (Adams and Richardson, 1960), up to 240 ppm (average 57.0 ppm) in the Lijiatian bauxite deposit in western Hunan Province, China (Xiao, 1960), up to 32.2 ppm in the Songqi bauxite deposit in Henan Province, China (Wang et al., 2012), up to 39.6 ppm in the Xinmu-Yanxi bauxite deposit (Huang et al., 2014) and up to 62.4 ppm in the Yunfeng bauxite deposit (Long et al., 2017) in northern Guizhou Province (China), and up to 36.3 ppm in the Bolkardağı bauxite deposit, Turkey (Hanilçi, 2013) (Table 1). As uranium is a mobile element at oxidizing conditions on the earth surface and its deposition generally takes place in relatively reducing environments (Cuney, 2009; Cumberland et al., 2016), and bauxite forms by intensive weathering and leaching on the earth surface, the uranium enrichment in bauxite is enigmatic. It is of both scientific and economic interest to investigate how uranium became enriched in the bauxite ores.

* Corresponding author.
E-mail address: Guoxiang.chi@uregina.ca (G. Chi).

https://doi.org/10.1016/j.gexplo.2018.04.010
Received 15 December 2017; Received in revised form 18 March 2018; Accepted 19 April 2018
Available online 25 April 2018
0375-6742/

Table 1
Examples of uranium enrichment in bauxite deposits.

Deposit name	Sample number	Min	Max	Average	Enrichment factor	Major source rocks	Reference
29 bauxite deposits (worldwide)		2.7	26.7	11.4	4.1	U contents of the ores related to the type of source rocks, with nepheline syenites having the highest and basic igneous rocks having the lowest U contents	Adams and Richardson (1960)
Lijiatian (Hunan, China)	107	10.5	240.0	57.0	20.4	Cambrian "Black Rock Sequence" shales	Xiao (1960)
Songqi (Henan, China)	17	6.8	32.2	18.0	6.4	Pre-Carboniferous argillaceous and carbonate rocks	Wang et al. (2012)
Xinmu-Yanxi (Guizhou, China)	16	6.3	39.6	17.4	6.2	Silurian Hanjiadian Formation shales	Huang et al. (2014)
Bolkardağı (Turkey)	47	3.5	36.3	12.5	4.5	Triassic pelitic rocks and shales	Hanilçi (2013)
Yunfeng (Guizhou, China)	17	18.0	62.4	35.1	12.5	Cambrian carbonates and "Black Rock Sequence" shales	Long et al. (2017)

Enrichment factor = Average of the samples/average of the upper continental crust (2.8 ppm; from Taylor and McLennan, 1985).

In a previous study of the Yunfeng paleo-karstic bauxite deposit (Long et al., 2017), it was found that the bauxite ores contain 18.0–62.4 ppm (average 35.1 ppm) U. The deposit is developed in Lower Carboniferous mudrocks above a karstic surface, which is underlain by Middle to Upper Cambrian carbonate rocks. Based on the elevated concentrations of U in the bauxite ores and its correlations with various immobile elements (Th, Zr, Nb, Ti, Al), it was concluded that the bauxite ores did not result from in-situ weathering of the dolomite underlying the orebodies, but rather from weathering of Lower Cambrian black shales that were exposed on the surface tens of kilometers away from Yunfeng (Long et al., 2017). It was inferred that the uranium in the bauxite ores was largely inherited from the black shales, but it remains unclear how the uranium survived the intensive weathering and leaching processes and in what forms it resides in the bauxite ores.

In this paper, we carried out petrographic, electron probe micro-analyzer (EPMA) and Raman spectroscopic studies of 17 bauxite ores from the Yunfeng deposit in order to determine the status of uranium in the bauxite ores. Furthermore, using the newly obtained mineralogical (EPMA and Raman) data together with the geochemical data reported in Long et al. (2017), we examined the possible mechanisms and processes of uranium mobilization and fixation during the formation of bauxite ores. The significance of the study results for understanding the behavior of uranium in weathering and diagenesis, the implications for uranium mineralization in sedimentary basins in general, as well as for exploitation of bauxite ores as a potential uranium resource, is discussed.

2. Regional geology and geological characteristics of the Yunfeng deposit

The Yunfeng bauxite deposit is located in central Guizhou Province, southwestern China (Fig. 1a). It is one of many bauxite deposits distributed in three major areas in the region, i.e., Xiuwen – Qingzhen, Zhengan – Daozhen and Kaili – Huangping (Fig. 1a). These bauxite areas are associated with the Qianzhong Uplift (Fig. 1a), which was formed through multiple tectonic events. The first tectonic event is the late Cambrian Yunan orogeny, which uplifted the marine strata that were formed from Sinian (Neoproterozoic) to late Cambrian and resulted in local development of paleo-lands (Guizhou Bureau of Geology and Minerals, 1987; Mei et al., 2006). The central Guizhou region was further uplifted in the subsequent Duyun orogeny in the Ordovician, which resulted in exposure of the Cambrian strata (Fig. 1b) for > 100 million years (Deng et al., 2010; Ling et al., 2015), until the deposition of early Carboniferous sedimentary rocks in relation to the transgression of the paleo-South China Sea (Guizhou Bureau of Geology and Minerals, 1987; Liu, 2001; Ling et al., 2015). The region was subsequently uplifted again during the Ziyun Movement in Late Carboniferous, followed by a transgression in Middle Permian forming marine carbonate sedimentation. The region was then subject to the Dongwu orogeny in late Permian to early Triassic, which is recorded by the unconformity between Lower Triassic and Permian rocks (Guizhou Bureau of Geology and Minerals, 1987).

The strata in the Xiuwen-Qingzhen bauxite area, in which the Yunfeng bauxite deposit is located (Fig. 1a), consists of the Sinian Dengying Formation, Lower Cambrian Niutitang, Mingxinsi, Jindingshan, and Qingxudong formations, Middle-Upper Cambrian Gaotai, Shilengshui formations and Loushanguan Group, Lower Carboniferous Jiujialu and Baizuo formations, Permian Liangshan, Qixia and Maokou formations, and Lower-Triassic Daye Formation (Fig. 2). Of particular interest to this study are the Jiujialu Formation that hosts the bauxite deposits in the area, the Liangshan Formation that unconformably overlies the Jiujialu Formation, and the Loushanguan Group that unconformably underlies the Jiujialu Formation (Fig. 2). Also of importance for this study is the Niutitang Formation black shales, which have been inferred to be the source rocks of the bauxite ores (Long et al., 2017). The Liangshan Formation is a thin (0–18 m) interval made of carbonaceous shales, and the Jiujialu Formation consists of mudstone, claystone and bauxite ores, whereas the Loushanguan Group is mainly composed of dolomite (Fig. 2). The Jiujialu Formation is transitional to the Baizuo Formation that is comprised of argillaceous dolomite. The Lower Cambrian Niutitang Formation and equivalents, known as the "Black Rock Sequence" that is widely distributed in South China, is rich in U, Pb, Ni, Sb, Cu, Mo, Fe, P, REE and V (Yang et al., 2013; Pi et al., 2013; Wang and Zhang, 2016; Zhang et al., 2017). The concentrations of U range from 23.3 to 102.4 ppm for the "Black Rock Sequence" in the central part of the Qianzhong Uplift, which is characterized by development of pyrite, organic matter, phosphatic nodules and Ni-Mo-V mineralization (Fig. 1b; Wang and Zhang, 2016). Many uranium minerals such as pitchblende, coffinite and brannerite have been found in this stratigraphic interval in South China (Zhao et al., 2014; Pi et al., 2013).

The Yunfeng bauxite deposit occurs in the northwest of the Xiuwen-Qingzhen bauxite area (Fig. 1a). The orebodies occur as a thin layer (average 5.8 m) within the Jiujialu Formation, which is sandwiched between the Loushanguan Group and the Liangshan Formation (Fig. 2). The Jiujialu Formation is divided into three layers as shown in Fig. 2a: an upper layer of bauxitic claystone, a middle layer of bauxite ores and a lower layer of bauxitic claystone. The bauxite ores exhibit various colors from light grey to dark grey and have earthy, massive, pisolitic and oolitic as well as clastic structures (Fig. 3).

3. Samples and analytical methods

Seventeen (17) bauxite ore samples (Al_2O_3 > 50 wt%) were collected from both outcrops and underground tunnels of the Yunfeng deposit (Fig. 2b). The samples were analyzed for mineral components and major and trace element compositions using X-ray diffraction (XRD), electron probe micro-analyzer (EPMA), wet chemistry method, and inductively coupled plasma – mass spectrometry (ICP-MS). The

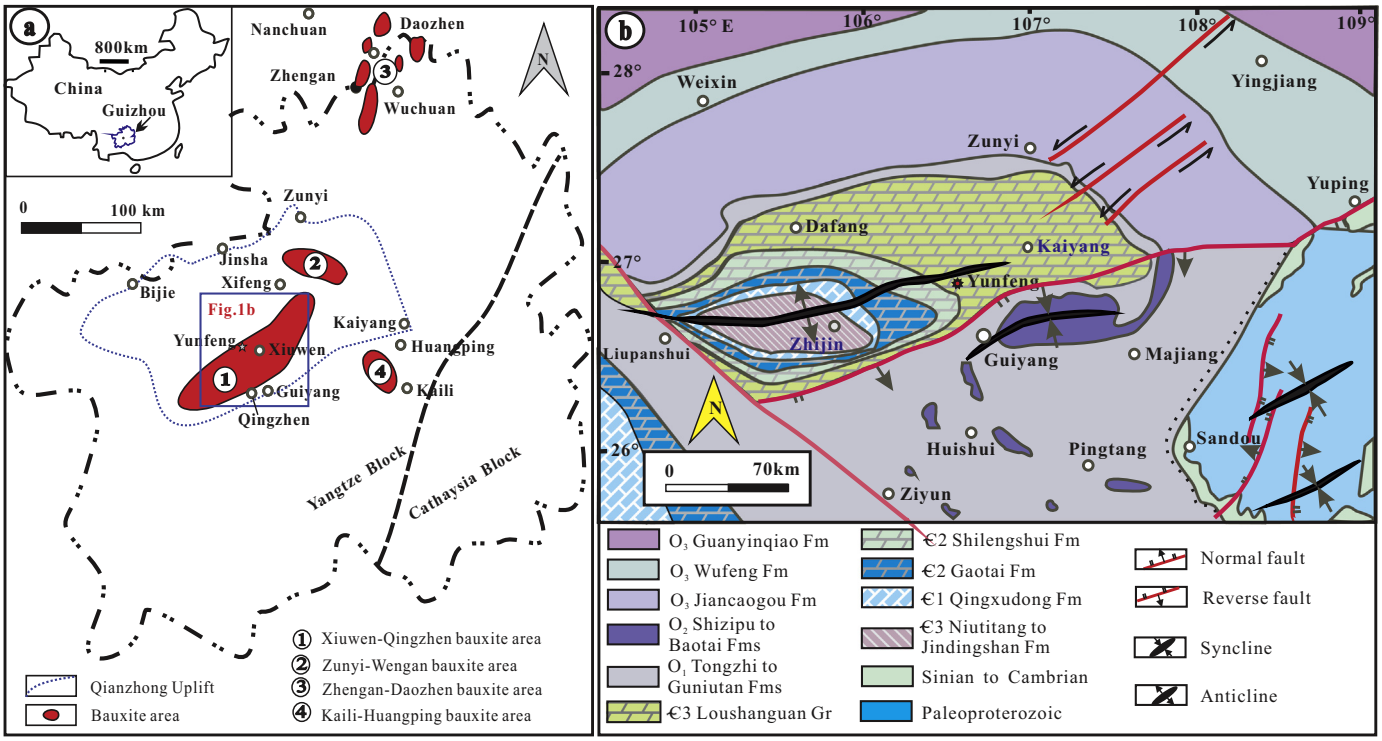

Fig. 1. (a) Sketch map showing the distribution of bauxite areas in Guizhou province in South China (modified from Li et al., 2014); (b) Paleo-structural map of the Qianzhong Uplift in Ordovician in relation to the Duyun Movement (modified from Deng et al., 2010).

XRD, EPMA and ICP-MS analyses were conducted at the School of Geosciences and Info-Physics, Central South University, and the wet chemistry analysis was performed at the Analytical Detection Central of the Changsha Research Institute of Mining and Metallurgy, Hunan, China.

The XRD studies were performed with a Rigaku D/Max-2200 model instrument using a Cu Kα tube with settings of 40 kV and 20 mA; the scanning scope, step length and speed were set to 2°–60°, 0.04° and 10°/

Series	Formation (Group)	Thickness (m)	Lithologies
Lower Triassic	Daye	0-647	Limestone, marlstone
Middle Permian	Maokou	0-372	Limestone, dolomite
	Qixia	93-178	Limestone
	Liangshan	0-18	Shale, mudrock
Lower C	Jiujialu / Baizuo	0-15	Mudrock, clay, bauxite
Middle -Upper Camb	Loushanguan	0-1035	Dolomite
	Gaotai-Shilengshui	0-226	Dolomite, sandstone, shale
Lower Camb	Qingxudong	181-338	Dolomite, sandstone
	Jindingshan	151-397	Sandstone, siltstone
	Mingxinshi	183-398	Sandstone, siltstone, mudrock
	Niutitang IV	12-308	Black shale, siltstone
	Niutitang III		Black shales, Ni–Mo–V
	Niutitang II		Claystone, tuff
	Niutitang I		Siliceous phosphorite
Upper Sinian	Dengying		Dolomite

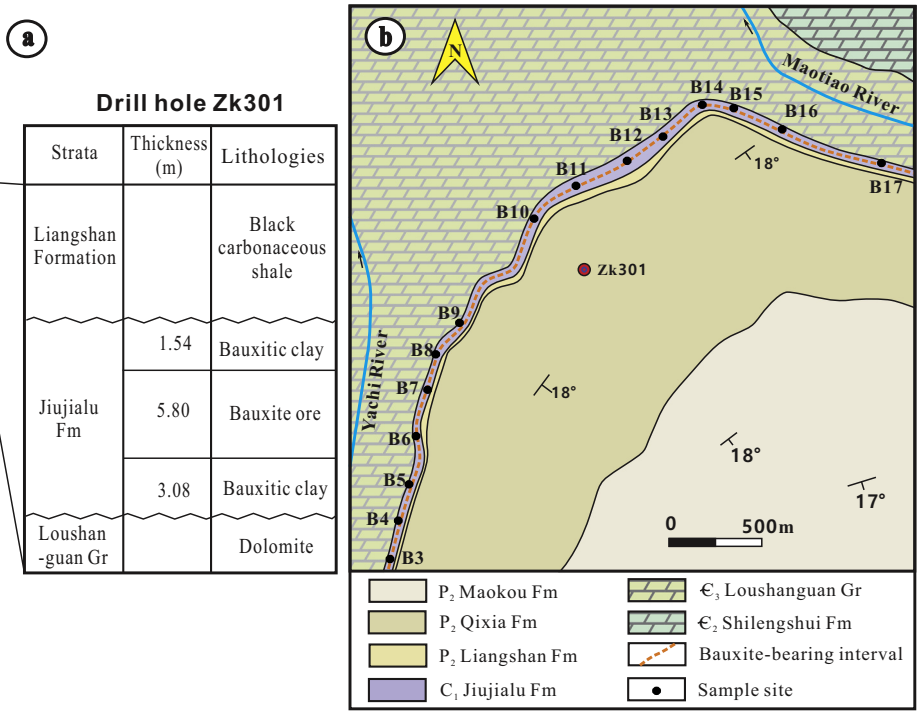

Fig. 2. (a) Stratigraphic column of the Xiuwen – Qingzhen area (modified from Guizhou Bureau of Geology and Minerals, 1987; Pi et al., 2013; Yang et al., 2013; Wang and Zhang, 2016) and that of the Yunfeng bauxite deposit as shown by the drill hole ZK301 (modified from Yunfeng Mining Company, unpublished data, 2013); (b) Geological map of the Yunfeng bauxite deposit showing the locations of samples examined in this study (modified from Yunfeng Mining Company, unpublished data, 2013).

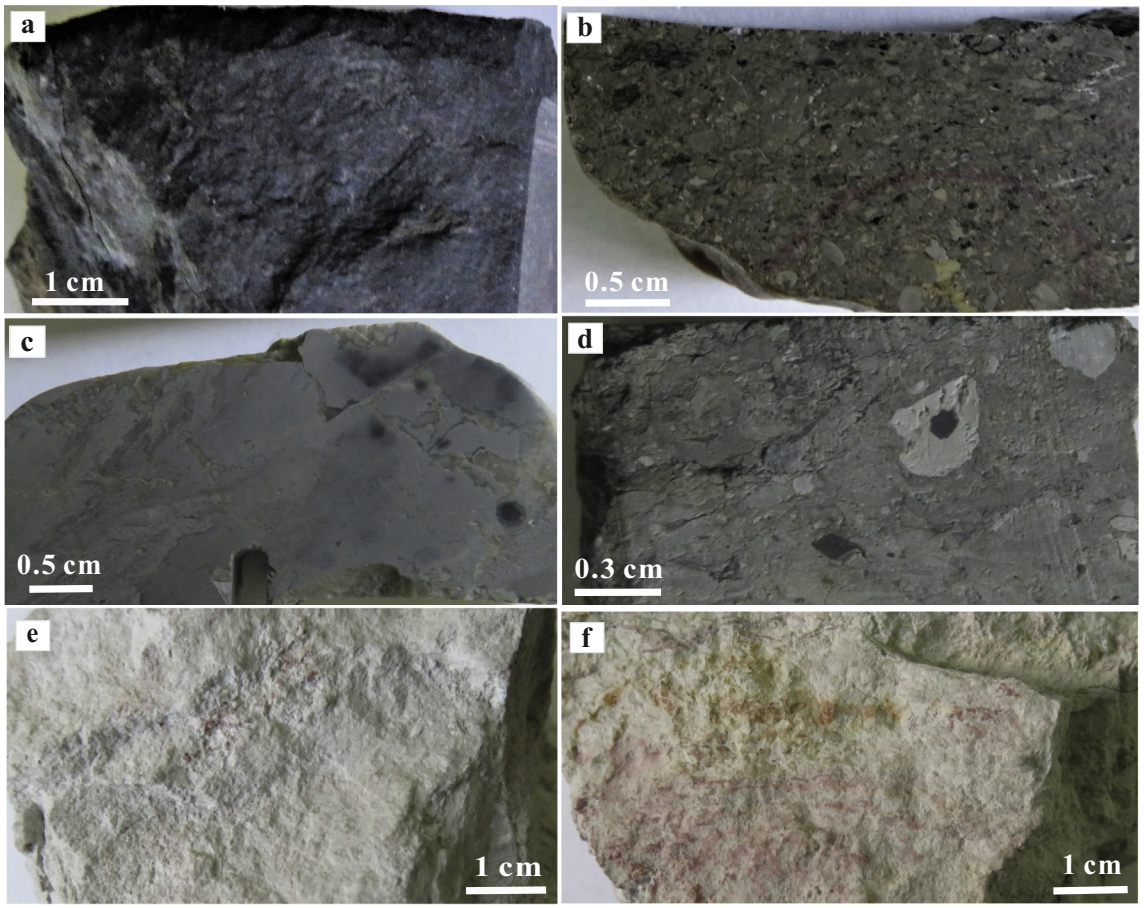

Fig. 3. Photos of bauxite ores from the Yunfeng deposit showing various colors and structures. (a) Dark grey massive bauxite; (b) Grey pisolitic and oolitic bauxite; (c) Grey massive bauxite; (d) Grey clastic bauxite; (e) Light grey earthy bauxite; (g) Grayish pink earthy bauxite. (For interpretation of the references to colour in this figure legend, the reader is referred to the web version of this article.)

Table 2
Mineral components (wt%), major elements (wt%) and U and related trace element concentrations (ppm) of bauxite ores from the Yunfeng deposit.[a]

Sample #	B1	B2	B3	B4	B5	B6	B7	B8	B9	B10	B11	B12	B13	B14	B15	B16	B17	Avg.
Diaspore	82.85		78.51	47.04	84.81				78.21		82.75	63.91	80.56	63.33		60.61	67.05	71.78
Illite	7.85		5.44	42.49	6.55				4.26		4.13	26.87	5.98	24.77		27.51	19.37	15.93
Kaolinite	2.4		3.16	0.34	1.58				1.14		4.89	1.02	4.96	0.08		1.75	2.69	2.18
Hematite	0.97		2.37	0.09	1.65				6.57		3.91	1.79	2.6	2.47		1.37	1.75	2.32
Chamosite	1.46		1.43	5.39	1.53				3.66			3.07		3.13		3.01	2.15	2.26
Rutile	3.5		3.76	3.66	3.06				5.06		3.56	2.55	4.78	2.96		2.16	4.16	3.56
Anatase	0.73		0.2	0.32	0.44				0.24		0.42	0.51	0.37	0.07		0.16	0.18	0.33
Quartz			4.88		0.2				0.24				0.58	2.73		3.15	2.19	1.27
Gypsum	0.24		0.25	0.67	0.18				0.62		0.34	0.28	0.17	0.46		0.28	0.46	0.36
Al_2O_3	73.03	55.22	68.88	56.75	73.66	52.75	51.49	51.1	67.49	58.65	70.39	64.95	72.9	64.72	55.02	63.12	66.21	62.73
Fe_2O_3	1.11	2.37	2.2	2.4	1.69	2.49	23.49	2.23	6.77	5.54	3.69	2.57	1.77	3.06	5.91	2.26	2.14	4.22
SiO_2	1.78	24.24	7.21	19.07	2.05	21.79	21.32	24.4	1.97	15.76	1.56	11.99	2.34	11.97	18.92	12.62	8.92	12.23
TiO_2	4.23	1.92	3.96	3.98	3.5	5.11	2.6	2.2	5.3	3.22	3.98	3.06	5.15	3.03	2.58	2.32	4.34	3.56
P_2O_5	0.63		0.63	0.10	0.31				0.89		0.61	0.36	0.66	0.22		0.30	1.15	0.52
Zr	836	380	1240	1210	1090	4130	1110	996	847	737	847	1050	997	1050	870	1040	1210	1158
U	46.8	20.9	32.8	35.3	35.9	32.2	21.2	24	58.4	31.5	39.4	26.4	62.4	49.5	18.9	18	43.2	35.11
Th	134	81.9	106.5	72.3	93.9	62.8	56.2	50.3	178.5	93.1	124.5	76	179.5	75.1	42.1	59.3	143	95.82
Th/U	2.86	3.92	3.25	2.05	2.62	1.95	2.65	2.10	3.06	2.96	3.16	2.88	2.88	1.52	2.23	3.29	3.31	2.73
Ce/Ce[a]	0.77	0.69	0.79	0.80	0.82	0.88	1.41	1.08	0.70	0.80	0.75	0.99	0.75	1.03	0.88	0.92	0.80	0.87

[a] Data source: Long et al. (2017); no XRD analysis was conducted for some of the samples that have low Al_2O_3 contents (B2, B6–8, B10, B15).

min, respectively. Semi-quantitative estimation of mineral components was conducted using the K value method. The EPMA analysis was performed using a Shimadzu EPMA-1720H electron probe micro-analyzer equipped with a wavelength dispersive spectrometer (WDS) and EDAX Genesis energy dispersive spectrometer (EDS). Silicates, oxides, and pure elements were used as standards (analytical errors are 1% for major elements and 3% for minor elements). Back scattered electron images were obtained at an accelerating voltage of 12 kV and a beam current of ~10 μA.

Trace elements were analyzed with a Thermo Electron Corporation VG PQ EXCELL ICP-MS. The analytical procedures are detailed in Long et al. (2017). The relative standard deviation (RSD) of the trace

elements analysis was below 4%. Major elements (Al_2O_3, Fe_2O_3, SiO_2, TiO_2 and P_2O_5) of the samples were determined by a wet chemistry method using the parallel samples and international standard samples (GBW07179, GBW07405) for data quality control, with precision better than 5%.

Selected minerals were analyzed with Raman spectroscopy. The analysis was conducted in the Geofluids Lab at the Department of Geology, University of Regina, with a Renishaw RM2000. The excitation laser wavelength is 514 nm, the grating is 1800, and the objective is ×50. The acquisition time is 30 s.

4. Results

XRD analyses indicate that the bauxite ores are mainly composed of diaspore (47.0 to 84.8 wt%, avg. 71.8 wt%) and illite (4.1 to 42. wt%, avg. 15.9 wt%), with minor amounts of kaolinite (0.1 to 5.0 wt%, avg. 2.2 wt%), hematite (0.1 to 6.6 wt%, avg. 2.3 wt%), chamosite (0 to 5.4 wt%, avg. 2.3 wt%), rutile (2.2 to 5.1 wt%, avg. 3.6 wt%), anatase (0.1 to 0.7 wt%, avg. 0.3 wt%), quartz (0 to 4.9 wt%, avg. 1.3 wt%), and gypsum (0.2 to 0.7 wt%, avg. 0.4 wt%) (Table 2). Trace amounts of zircon, xenotime, pyrite, stibnite, chalcopyrite, galena, Ni-Co-rich arsenopyrite - glaueodot, Ni-Co-rich pyrite and uranium-bearing minerals were also detected by EPMA and SEM-EDS as well as Raman analyses. The U concentrations of the bauxite ores range from 18.0 to 62.4 ppm with an average of 35.1 ppm (Table 2).

Diaspore is dispersed in (Fig. 4a) or interweaved with (Fig. 4b) illite, whereas rutile (Fig. 4a) and zircon (Fig. 4b) occur as detrital grains scattered in the matrix of illite, kaolinite and diaspore. Chamosite is associated with illite and may occur as relatively coarse crystals dispersed in the matrix of illite (Fig. 4b). Pyrite occurs in two forms: framboidal pyrite and subhedral to euhedral pyrite. Framboidal pyrite commonly occurs as aggregates in the matrix of kaolinite (Fig. 4c), and subhedral to euhedral pyrite as well as other sulfides such as chalcopyrite are dispersed in diaspore (Fig. 4d). EPMA analysis indicates that the subhedral to euhedral pyrite may contain significant and variable amounts of Ni, Co and As (Figs. 4e–h), whereas framboidal pyrite does not contain these elements. Other sulfide and sulfosalt minerals, including stibnite, galena and Co-Ni-rich arsenopyrite – glaueodot, have similar occurrences as subhedral and euhedral pyrite and chalcopyrite, i.e., dispersed in diaspore, illite and kaolinite. EPMA data (Fig. 4e–g) and element mapping (Fig. 4h) indicate that Ni-Co-rich pyrite and Ni-Co-rich arsenopyrite exist as distinct mineral phases, and within each of them there are significant compositional changes (Fig. 4h), suggesting presence of separate S-As-Fe-Co-Ni minerals (e.g. glaueodot, (Co,-Fe)AsS) as sub-micron-scale inclusions.

Uranium-bearing mineral(s) are commonly associated with Ti-oxides (rutile and anatase) and sulfides (especially pyrite) (Figs. 5a to d). The U-bearing mineral(s) occur as micron- to submicron-sized grains rimming the anatase (Figs. 5a and 6), filling micro-cracks in kaolinite near pyrite (Fig. 5b), and disseminations in kaolinite as well as diaspore in close association with pyrite (Figs. 5c and d). EPMA analysis indicates that the U-bearing mineral(s) are rich in U and O (Figs. 5e and f), with UO_2 contents ranging from 38.96 to 70.45 wt%. Other elements detected by EPMA include Ti, Al, Si, Fe, S, As, P, Ni, Zr, Pb, Co and V.

Because of the small size of the U-bearing mineral(s), the EPMA results likely reflect mixtures of the U-bearing mineral(s) and the matrix or surrounding minerals, and therefore cannot be used to identify the mineral(s). Furthermore, the contents of uranium mineral(s) are too low to be detected by XRD. However, Raman spectroscopy is able to separate signals from closely spaced minerals, as shown by the example of Fig. 5a, where the Raman bands for the U-bearing mineral and anatase are clearly separated (Figs. 5g and h). The Raman peaks detected at around 442 cm^{-1} and 606 cm^{-1} (Fig. 5g) as well as at around 454 cm^{-1} suggest that the main U-bearing mineral may be uraninite (Xiao et al., 2012; Palacios and Taylor, 2000). Nevertheless, it is possible that other uranium minerals such as UO_{2+x} micro to nanocrystals (Klinkhammer and Palmer, 1991; Myllykylä, 2008; Cumberland et al., 2016; Bonnetti et al., 2017) are present.

The paragenetic sequence of the minerals found in the bauxite ores are summarized in Fig. 7, based on occurrences of the minerals and their crosscutting relationships. Quartz, zircon, rutile and anatase are detrital grains inherited from the precursor rocks of the bauxite ores. The positive correlation between rutile and diaspore (Fig. 8a) suggests co-enrichment of resistant residual minerals and aluminum hydroxides during the weathering process. Fe-oxides were likely the products of weathering, together with gibbsite, boehmite and kaolinite. However, gibbsite and boehmite appear to have been completely converted to diaspore, whereas kaolinite was partially converted to illite in the diagenetic stages. The negative correlation between kaolinite and illite (Fig. 8b) supports this interpretation. Framboidal pyrite is interpreted to have formed mainly in the early diagenesis stage, perhaps with UO_{2+x} nanocrystals, whereas uraninite, chamosite, illite, diaspore, subhedral to euhedral pyrite as well as other sulfides and sulfosalts were mainly formed in the burial diagenetic stage (Fig. 7).

A broad positive correlation is observed between U and Al_2O_3 contents (Fig. 8c), and to a lesser extent between U and diaspore contents (Fig. 8d). A clear positive correlation exists between U and TiO_2 contents (Fig. 8e) as well as between U and rutile contents (Fig. 8f). A vague positive correlation is also observed between U and P_2O_5 (Fig. 8g). In contrasts, there appears to be no correlation between U and Fe_2O_3 (Fig. 8h), illite (Fig. 8i), and Zr (Fig. 8j).

5. Discussion

The U concentrations in the bauxite ores from the Yunfeng deposit (18.0 to 62.4 ppm, average 35.1 ppm) are significantly higher than the crustal values (approximately 1 to 3 ppm, Taylor and McLennan, 1985; Cumberland et al., 2016). It is of both scientific and economic significance to understand the mechanisms of uranium enrichment in the bauxite ores. Uranium occurs in nature in two main valence states, U^{4+} and U^{6+} (Burns, 1999), and its solubility is much higher in the U^{6+} than the U^{4+} state (Langmuir, 1978; Romberger, 1984; Cuney, 2009; Skirrow et al., 2009; Fayek, 2013; Cumberland et al., 2016). As a result, uranium is generally leached in oxidizing conditions and precipitated in reducing environments (Cuney, 2009; Skirrow et al., 2009; Yang et al., 2009; Fayek, 2013; Cumberland et al., 2016).

Karstic bauxite deposits form as a result of aluminosilicate minerals being subjected to intense chemical weathering (laterization), transportation, deposition and/or further laterization and diagenesis in depressions and karstic holes under tropical to subtropical climatic conditions (Bárdossy and Aleva, 1990; Hanilçi, 2013; Zhang et al., 2013; Ling et al., 2015; Ahmadnejad et al., 2017). Because the weathering takes place on the earth surface, which is generally oxidizing, it would be expected that uranium was leached rather than precipitated during the formation of bauxite ores. However, the positive correlation between U and Al_2O_3 (Fig. 8c) suggests that the more weathering the precursor rocks experienced (thus higher Al_2O_3), the more uranium is enriched. This is contradictory with the prediction that more uranium will be leached with increasing degree of weathering at oxidizing conditions. Such a paradox suggests that either the formation of the bauxite did not happen in an oxidizing environment, or the bauxite ores have a mechanism to trap uranium that may counteract the effect of uranium leaching due to oxidizing condition. In order to evaluate these potential mechanisms, we need to examine the status of uranium in the bauxite ores first.

Uranium in rocks can occur as separate U-minerals (e.g. uraninite and coffinite), lattice substitutions in accessory minerals (e.g., apatite and zircon), and in exchangeable sites in or adsorbed onto the surfaces of zeolite, clay minerals and oxide minerals (Richardson, 1959; Burns, 1999; Skirrow et al., 2009; Bachmaf and Merkel, 2010; Li et al., 2013; Fayek, 2013; Bonnetti et al., 2015, 2017; Cumberland et al., 2016; Akhtara et al., 2017). The positive correlations between U and Al_2O_3 or

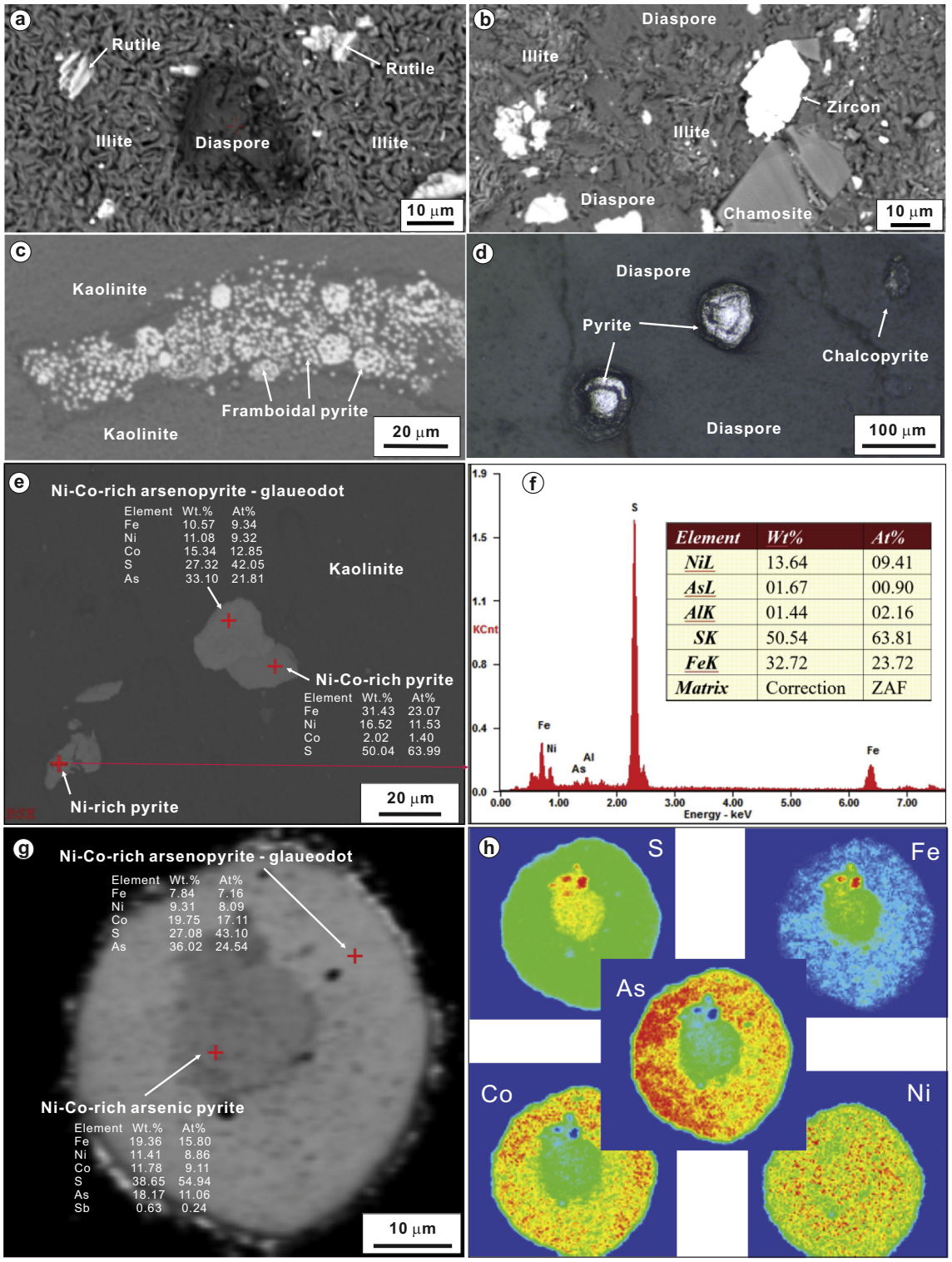

Fig. 4. Backscattered electron (BSE) images showing: (a) diaspore and detrital rutile dispersed in illite; (b) detrital zircon, together with chamosite and diaspore, occurring in the matrix of illite; (c) aggregates of framboid pyrite occurring in the matrix of kaolinite; (d) anhedral to subhedral pyrite, together with chalcopyrite, occurring in the matrix of diaspore; (e) anhedral Ni-Co-rich pyrite and Ni-Co-rich arsenopyrite – glaueodot occurring in the matrix of kaolinite; EPMA data shown for selected spots; (f) energy spectrum of a Ni-rich pyrite shown in (e); (g) Ni-Co-rich arsenic pyrite enclosed by Ni-Co-rich arsenopyrite – glaueodot; EPMA data shown for selected spots; (h) element mapping of the minerals shown in (g).

diaspore (Figs. 8c and d), and between U and TiO_2 or rutile (Figs. 8e and f), suggest that uranium may have been adsorbed to the Al-hydroxides (gibbsite and boehmite) and Ti-oxides (rutile and anatase). However, the positive correlation between rutile and diaspore (Fig. 8a) and the occurrences of U-minerals in close association with anatase (Figs. 5a and 6) imply that U may be more likely adsorbed to Ti-oxides than to Al-hydroxides. The poor correlations between U and Fe_2O_3 (Fig. 8h), illite (Fig. 8i) and Zr (Fig. 8j) indicate that U adsorption on Fe-oxides/hydroxides and clay minerals, and U contained in zircon, are unimportant for U enrichment in the bauxite. The uranium in the

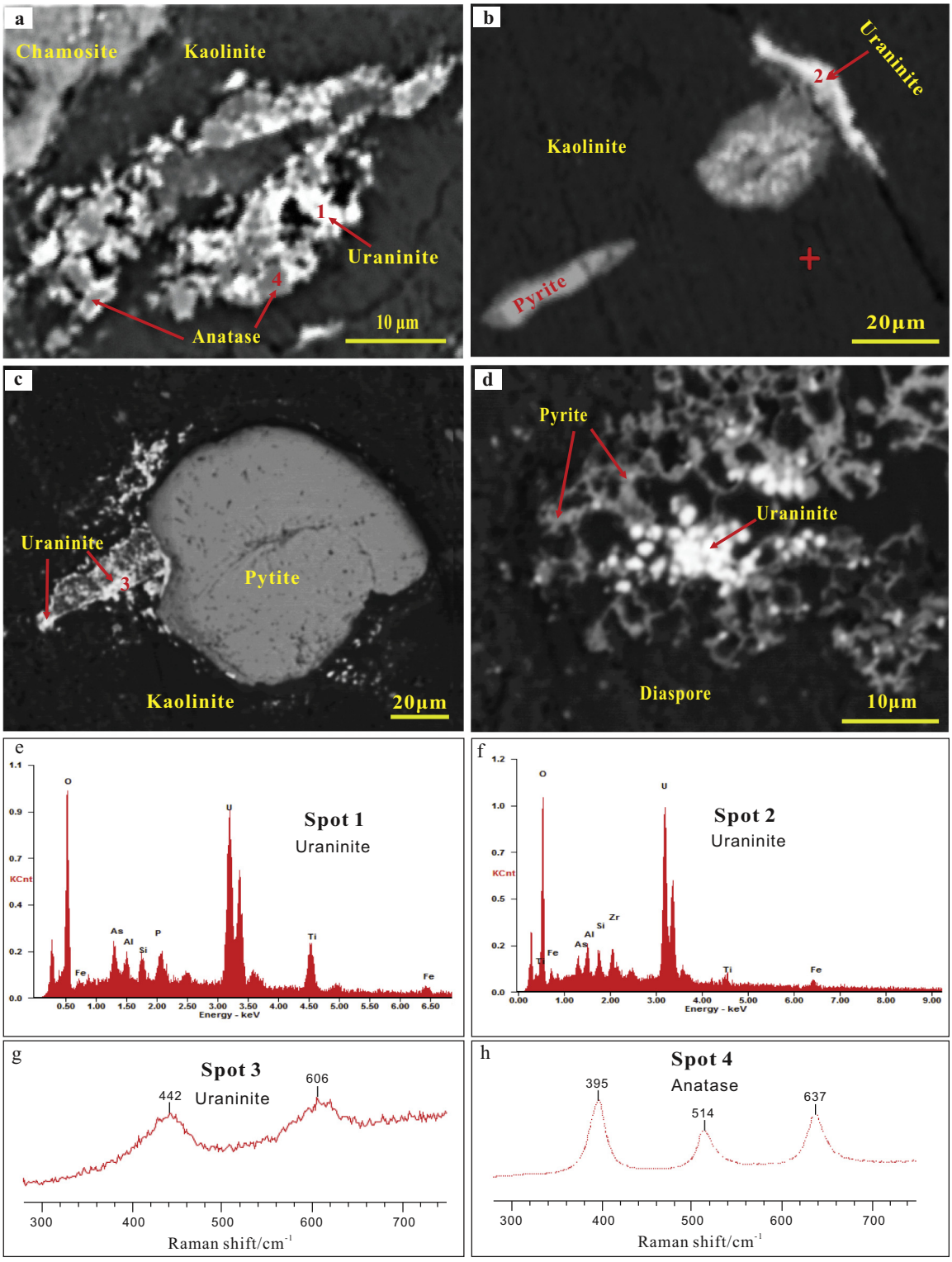

Fig. 5. Backscattered electron (BSE) images showing: (a) uraninite rimming anatase in the matrix of kaolinite; (b) uraninite filling a micro-crack in kaolinite; (c) uraninite disseminated in kaolinite and close to an anhedral pyrite crystal; (d) uraninite disseminated in diaspore in close association with pyrite; (e) energy spectrum of a U-mineral (spot 1 in a) associated with anatase; (f) Energy spectrum of a U-mineral (sport 2 in b); (g) Raman spectra of a U-mineral (sport 3 in c); (h) Raman spectra of anatase (spot 4 in a).

bauxite ores probably mainly occurs as separate U-minerals (likely uraninite) associated with Ti-oxides and sulfides (Figs. 5 and 6).

The bauxite ores of the Yunfeng deposit have been inferred to form from weathering of black shales of the Lower Cambrian Niutitang Formation, which were transported from the central part of the Qianzhong Uplift (Fig. 1b) and deposited in karstic depressions in the Yunfeng area (Long et al., 2017) (Fig. 9a). Although running surface water may have resulted in an overall oxidizing condition, the organic matter and sulfides initially contained in the black shales likely created local (grain-scale) reducing environments. Thus, an evolving, dynamic

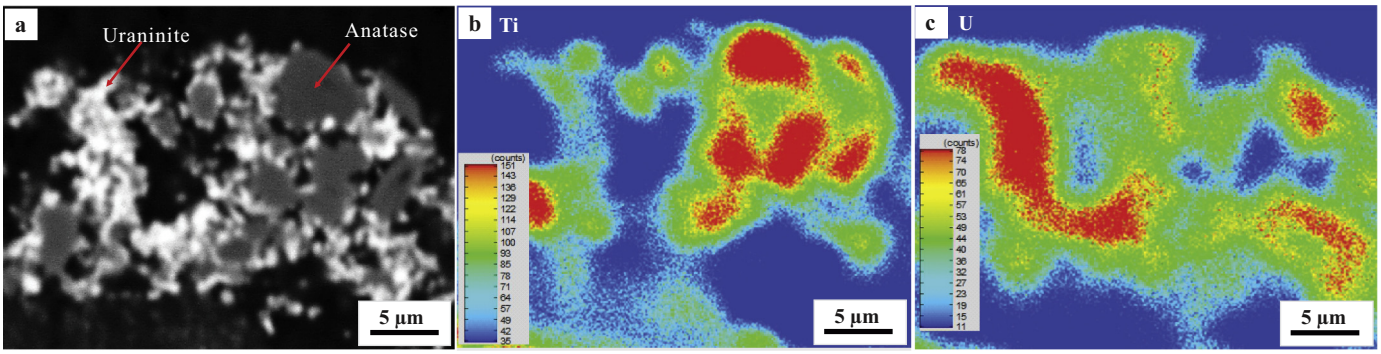

Fig. 6. (a) Backscattered electron (BSE) image showing a U-mineral rimming anatase; (b) Ti mapping of the area corresponding to the image shown in a; (c) U mapping of the area corresponding to the image shown in a.

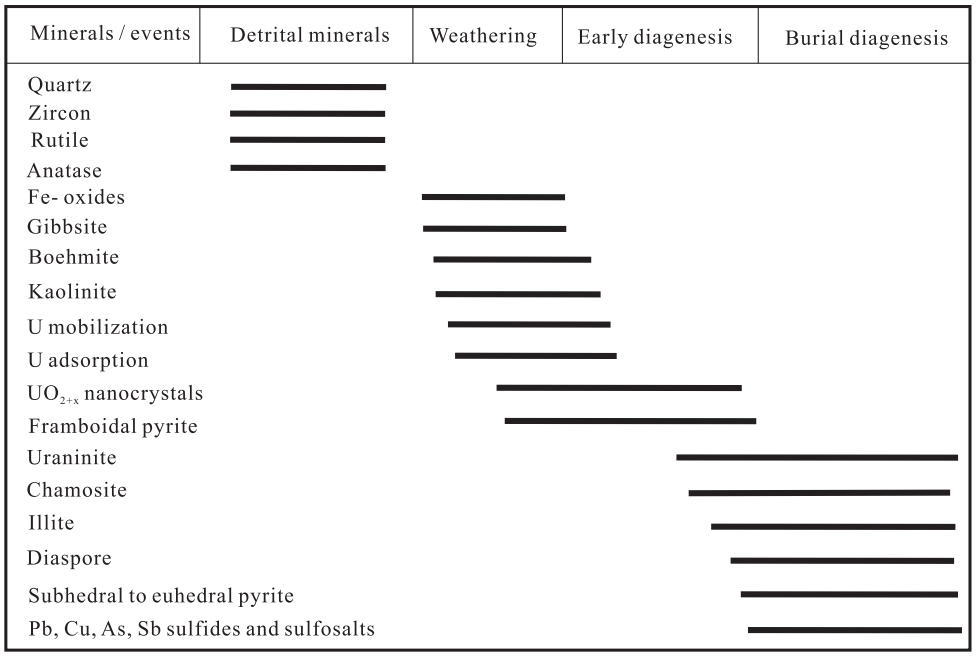

Fig. 7. Paragenetic sequence of the Yunfeng bauxite deposit.

redox system (both in time and space) may be envisaged during the bauxite formation of the Yunfeng deposit. Such an unsteady redox system may be reflected by Ce anomalies and Th/U ratios (Lukas et al., 1983; Pollack et al., 2009). Zhang et al. (2013) suggested that alternation of positive and negative Ce anomalies within a deposit may indicate changing redox environments during bauxite formation. Tao et al. (2009) suggested that Th/U ratios of < 2 indicate reducing depositional environments, and Th/U vales of > 7 indicate oxidizing depositional environments, whereas Th/U ratios between 2 and 7 suggest intermediate or transitional redox environments. The Ce/Ce* values (0.69 to 1.41) and Th/U values (1.52 to 3.92) of the bauxite ores from the Yunfeng deposit (Table 2) are consistent with the inference of the intermediate and variable redox conditions.

The variable redox conditions at the site of bauxite mineralization is favorable for the retention of uranium during chemical weathering. On one hand, uranium that was originally contained in the black shales were remobilized due to oxidation from U^{4+} to U^{6+} and were leached, especially in the vadose zone above the water table (Fig. 9b). The overall oxidizing conditions during the chemical weathering also resulted in oxidation of the polymetallic (Fe-, Ni-, Co-, Cu-, Sb- and Pb-) sulfides and sulfosalts that were originally enriched in the black shales (Yang et al., 2013; Pi et al., 2013; Wang et al., 2016; Zhang et al., 2017), producing an acidic solution rich in Fe^{3+}, Ni^{2+}, Co^{2+}, Cu^{2+}, Sb^{2+} and Pb^{2+} and SO_4^{2-} (Villar et al., 2002; Hou et al., 2017). Such a solution may accelerate the initial chemical weathering of aluminosilicate minerals to form kaolinite, and favor uranium dissolution as uranyl-sulfate complexes (Langmuir, 1978; Villar et al., 2002; Kyser and Cuney, 2009; Jaireth et al., 2015). As a result, U^{6+}, Fe^{3+} and $SO_4^{=}$, together with many other components originally contained in the shale, were leached from the upper part of the weathering profile (Fig. 9b). On the other hand, the ubiquitous presence of local reducing environments prevented uranium from being transported over long distance. In particular, in the lower part of the weathering profile below the water table, the U^{6+} was converted back to U^{4+} shortly after it was mobilized from the upper part, and may be trapped as UO_{2+x} nanocrystals that were adhered to Ti-oxides. At the same time, $SO_4^{=}$ leached from the upper part of the weathering profile was converted to reduced sulfur, resulting in the formation of framboidal pyrite (Fig. 9b), which typically forms at oxic-anoxic interface (Wilkin et al., 1996, 1997; Pisarzowaka et al., 2014; Gallego-Torres et al., 2015). Thus, UO_{2+x} nanocrystals and sulfides may be formed in the weathering stage (Fig. 9b), i.e., contemporaneously with the formation of bauxite ores, although they most likely would continue to form in the early diagenetic stage (Fig. 9c).

The bauxite ores that were formed in the chemical weathering stage were subsequently subjected to diagenesis with the start of the

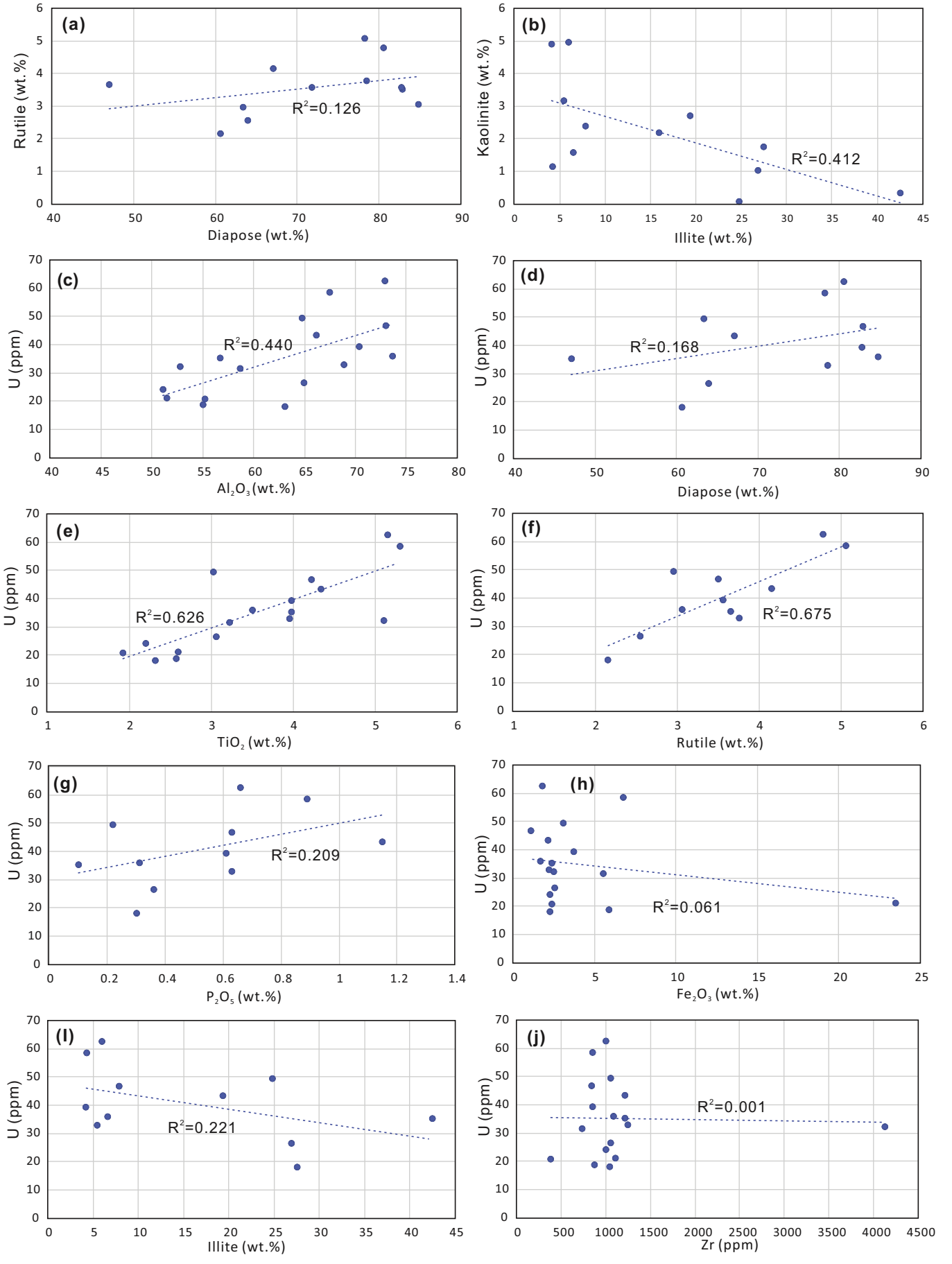

(caption on next page)

Fig. 8. Bivariant diagrams between various components of the bauxite ores of the Yunfeng deposit (data from Table 2). (a) rutile versus diaspore; (b) kaolinite versus illite; (c) U versus Al_2O_3; (d) U versus diaspore; (e) U versus TiO_2; (f) U versus rutile; (g) U versus P_2O_5; (h) U versus Fe_2O_3; (i) U versus illite; (j) U versus Zr.

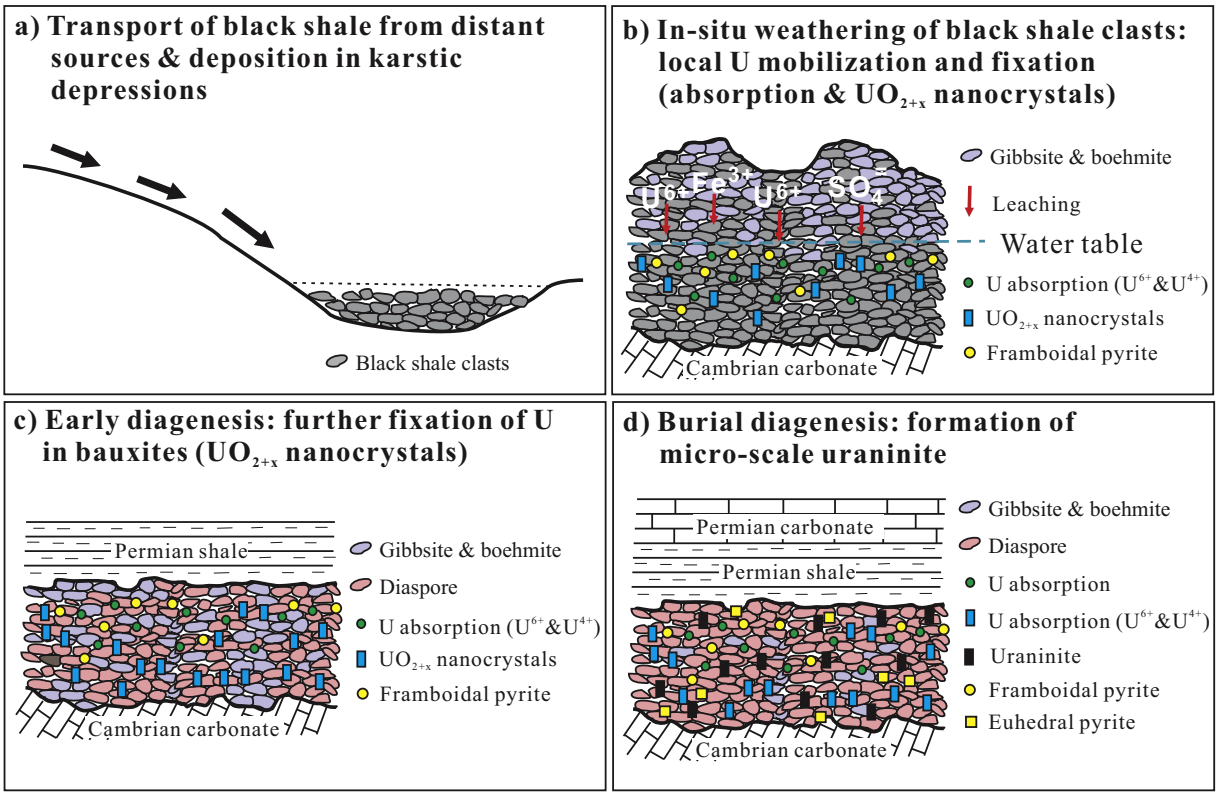

Fig. 9. A schematic model showing the processes of uranium enrichment in the Yunfeng bauxite deposit. a) transport and deposition of detrital clasts of black shales from the source to karstic depressions; b) in-situ weathering of the black shale clasts, with U^{6+}, Fe^{3+} and $SO_4^{=}$ and other components being leached from the upper part of the weathering profile (together with the formation of gibbsite and boehmite) and their refixation in the lower part of the profile; c) further fixation of the remobilized uranium and sulfur together with the transformation from gibbsite and boehmite to diaspore in early diagenesis; d) recrystallization and coarsening of uraninite and sulfides in burial diagenesis.

deposition of the Middle Permian Liangshan Formation (Fig. 9c), which is mainly composed of black carbonaceous shale (Fig. 2a). Thus, the overall redox condition changed from oxidizing (with local reducing) to reducing. In the early diagenesis stage, gibbsite and boehmite formed in the weathering stage (Kittrick, 1969; Panahi et al., 2000) started to be converted to diaspore (Fig. 9c), and this conversion continued in the burial diagenesis stage (Fig. 9d). The SO_4^{2-} in the pore fluid may be further transformed to H_2S and HS^- through bacterial sulfate reduction (BSR) and iron reducing bacteria (IRB) action (Pitkänen et al., 2004; Cumberland et al., 2016; Hou et al., 2017), and the pH value may increase (Mongelli, 1997; Pitkänen et al., 2004; Liu and Liao, 2014; Liu et al., 2017). Some of the Fe-oxides may be dissolved and the Fe^{2+} in the pore fluid may be increased, which may contribute to further formation of framboidal pyrite (Wilkin et al., 1996, 1997; Ling et al., 2015). Other metals (Ni^{2+}, Co^{2+}, Cu^{2+}, Sb^{2+} and Pb^{2+}) dissolved in the pore fluid may also react with S^{2-} to form sulfides and sulfosalts. Ni and Co could be incorporated into pyrite and form Ni- and Co-bearing arsenopyrite and/or pyrite because of their slower water-exchange kinetics than Fe, whereas Pb, Cu and Sb have faster water-exchange kinetics than that of Fe, and they are expected to form distinct sulfide phases (such as chalcopyrite, galena and stibnite) prior to the formation of pyrite (Morse and Luther, 1999; Botsou et al., 2015). At the same time, residual U^{6+} in the pore fluid may be further reduced to form UO_{2+x} nanocrystals (Klinkhammer and Palmer, 1991; Myllykylä, 2008; Cumberland et al., 2016; Bonnetti et al., 2017). In the burial diagenesis stage, with increasing temperature, gibbsite and boehmite were completely converted into diaspore (Kennedy, 1959) (Fig. 9d). Metal sulfides such as pyrite, chalcopyrite, galena and stibnite that formed in the early diagenesis stage were recrystallized to form coarser crystals, and the UO_{2+x} nanocrystals were also recrystallized to form microcrystals of uraninite (Fig. 9d).

The recognition of uraninite and its association with Ti-oxides and sulfides in the bauxite ores is important for potential exploitation of bauxite ores as a resource of uranium. The total proven and potential bauxite resource of Guizhou Province is up to 1 Bt (Mining120, 2017). Assuming an average of 35 ppm U in the ores, the total U resources contained in the bauxite ores in Guizhou (Fig. 1a) would be 35,000 t U. The possible extraction of uranium and other trace elements from bauxite residues have been discussed in several previous studies (Smirnov and Molchanova, 1997; Klauber et al., 2009; Liu and Naidu, 2014; Liu and Li, 2015).

Since uranium is present in uraninite in the bauxite ores, as in low-grade sandstone-hosted uranium deposits, the uranium extraction method used in the in-situ leaching mining of sandstone-hosted uranium deposits (Abzalov et al., 2014; Seredkin et al., 2016) might be borrowed for the utilization of uranium in bauxite ores or their residues. However, considering that the U concentrations in the bauxite ores are much lower than the minimum grade for economic exploitation of uranium (0.05% U for sandstone-hosted deposits; IAEA, 2009), much more work is warranted to understand the status of uranium in bauxite ores in order to effectively extract it.

On the other hand, our study results and the proposed uranium mobilization – fixation mechanisms have important implications for uranium exploration in sedimentary basins, especially for uranium

mineralization related to black shales. U-rich black shales in Cambrian strata are widespread in South China (Yang et al., 2013; Pi et al., 2013; Wang et al., 2016; Zhang et al., 2017), and they were exposed on the surface multiple times in the complex tectonic history of South China (Chen and Huang, 1990; Yao et al., 1998; Zhao, 2009; Ni et al., 2012). A number of uranium occurrences and uranium deposits have been found in association with black shales in southwestern China, including stratigraphic intervals in Upper Sinian – Lower Cambrian, Silurian, Permian and Triassic successions (Ni et al., 2012). Examples of such uranium mineralization include the Baimadong uranium deposit in central Guizhou Province (Ni et al., 2012; Mo et al., 2016), the Dawan uranium deposit in southern Hunan Province (Zhao et al., 2014), the No.138 sand-related uranium deposit in Zhejiang Province (Tang, 2002), the Chanziping unconformity-related uranium deposit (Chen and Huang, 1990; Wang et al., 2002) and the Daxin carbonate-type uranium deposit in Guangxi Province (Yao et al., 1998). However, most of the uranium deposits associated with the black shales are small, and the few large ones are generally related to multiple re-enrichments including supergene processes followed by hydrothermal events (Ni et al., 2012). Although not all the black shales that were once exposed on the surface were weathered to form bauxite ores, the paleo-weathering processes likely resulted in significant remobilization and enrichment of uranium in a similar manner as depicted in this study. The paleo-weathered black shales may be more porous and permeable than the original shales, and may become the site of further uranium mineralization if overprinted by hydrothermal activity. Thus, the intersections of paleo-weathered black shales with major structures connected with potential hydrothermal fluid sources may be potential exploration targets.

6. Conclusions

This study aims to document mineralogical characteristics of the uranium-rich Yunfeng paleo-karstic bauxite deposit and decipher the mechanism of uranium enrichment in the bauxite ores. The following conclusions may be drawn based on the research results.

1) The bauxite ores from the Yunfeng deposit are characterized by high contents of uranium (18 to 62 ppm, average 35 ppm). Separate U-minerals were indicated by EPMA and SEM-EDS analysis, and Raman spectroscopic analysis indicates that uraninite may be the dominant U-mineral. The U-minerals are closely associated with Ti-oxides and sulfides (especially pyrite).

2) There is a positive correlation between U and Al_2O_3 or diaspore, and between U and TiO_2 or rutile. There is no correlation between U and Fe_2O_3, illite, and Zr. These correlations suggest that U enrichment in the bauxite ores may be related to U adsorption with Ti-oxides (and perhaps with Al-hydroxides), but unrelated to adsorption with clay minerals and Fe-oxides as well as lattice substitution in residual zircon.

3) The Yunfeng bauxite ores were formed from weathering of shales of the Lower Cambrian “Black Rock Sequence”, which was originally enriched in organic matter, U and Fe-, Ni-, Cu-, Co- and As-sulfides. Weathering of such a protolith enriched in reducing agents (organic matter and sulfides) created variable local (grain-scale) oxidizing-reducing conditions in an overall oxidizing environment, where uranium originally adsorbed in the black shales were oxidized and leached, but shortly re-fixed as UO_{2+X} nanocrystals in association with Ti-oxides and sulfides.

4) The remobilization and re-precipitation of uraninite in the Yunfeng bauxite ores provide an example of potential uranium mineralization through weathering of U-rich black shales that are widespread in South China, the economic significance of which remains to be investigated.

5) The uranium enrichment mechanisms discussed in this paper may be applicable to other paleo-weathered black shales. Overprinting of such stratigraphic intervals by hydrothermal activity may lead to further uranium mineralization, which may represent potential uranium exploration targets.

Acknowledgments

We would like to thank Yang J.C. and Dr. Yang W. for assistance in the field work, and Prof. Gu X.P. for assistance in XRD, EPMA and SEM-EDS analysis and for discussion and suggestions during this study. This work was jointly supported by National Program on Key Basic Research Project (973 Program) (2015CB453002), Qingzhen Yunfeng Aluminum and Iron Mining Co. (738010033), the Innovation-driven Plan in Central South University (Grant 2015CX008), the National Natural Science Foundation of China (41672082, 41503037), and an NSERC-Discovery grant (to Chi). We are grateful to two anonymous JGE reviewers for their constructive reviews, which helped improve the quality of this paper. Editor Professor Stefano Albanese and Associate Editor Dr. Agustin Martin-Izard are thanked for handling the manuscript.

References

Abzalov, M.-Z., Drobov, S.-R., Gorbatenko, O., Vershkov, A.-F., Bertoli, O., Renard, D., Beucher, H., 2014. Resource estimation of in situ leach uranium projects. Appl. Earth Sci. 123, 71–85.
Adams, J.-A.-S., Richardson, K.-A., 1960. Thorium, uranium and zirconium concentrations in bauxite. Econ. Geol. 55, 1653–1675.
Ahmadnejad, F., Zamanian, H., Taghipour, B., Zarasvandi, A., Buccione, R., Ellahi, S.S., 2017. Mineralogical and geochemical evolution of the Bidgol bauxite deposit, Zagros Mountain belt, Iran: implications for ore genesis, rare earth elements fractionation and parental affinity. Ore Geol. Rev. 86, 755–783.
Akhtara, S., Yang, X., Pirajno, F., 2017. Sandstone type uranium deposits in the Ordos Basin, Northwest China: a case study and an overview. J. Asian Earth Sci. 146, 367–382.
Bachmaf, S., Merkel, B.J., 2010. Sorption and desorption of uranium (VI) on clay minerals. Clay in Natural & Engineered Barriers for Radioactive Waste Confinement, 4th International Meeting, March 2010. Nantes, France, pp. 391–392.
Bárdossy, G., Aleva, G.J.J., 1990. Lateritic Bauxites. Elsevier Scientific Publication, Amsterdam, pp. 1–624.
Bonnetti, C., Cuney, M., Malartre, F., Michels, R., Liu, X.D., Peng, Y.B., 2015. The Nuheting deposit, Erlian Basin, NE China: synsedimentary to diagenetic uranium mineralization. Ore Geol. Rev. 69, 118–139.
Bonnetti, C., Liu, X., Yan, Z., Cuney, M., Michels, R., Malartre, F., Mercadier, J., Cai, J., 2017. Coupled uranium mineralisation and bacterial sulphate reduction for the genesis of the Baxingtu sandstone-hosted U deposit, SW Songliao Basin, NE China. Ore Geol. Rev. 82, 108–129.
Botsou, F., Godelitsas, A., Kaberi, B., Mertzimekis, T.J., Goettlicher, J., Steininger, R., Scoullos, M., 2015. Distribution and partitioning of major and trace elements in pyrite-bearing sediments of a Mediterranean coastal lagoon. Chemie Der Erde-Geochem. 75, 219–236.
Burns, P.C., 1999. The crystal chemistry of uranium. Rev. Mineral. 38, 23–90.
Chen, Z.Y., Huang, S.J., 1990. On Meso-Cenozoic unconformity-related uranium deposits in Southeast China. Uranium Geol. 6 (5), 349–358 (in Chinese with English abstract).
Cumberland, S.A., Douglas, G., Grice, K., Moreau, J.W., 2016. Uranium mobility in organic matter-rich sediments: a review of geological and geochemical processes. Earth Sci. Rev. 159, 160–185.
Cuney, M., 2009. The extreme diversity of uranium deposits. Mineral. Deposita 44, 3–9.
Deng, X., Yang, K.G., Liu, Y.L., She, Z.B., 2010. Characteristics and tectonic evolution of Qianzhong uplift. Earth Sci. Front. 17 (3), 79–89 (In Chinese with English abstract).
Fayek, M., 2013. Uranium ore deposits: a review. Mineral. Assoc. Canada Short Course Series 43, 121–147.
Gallego-Torres, D., Reolid, M., Nieto-Moreno, V., Martínez-Casado, F.J., 2015. Pyrite framboid size distribution as a record for relative variations in sedimentation rate: an example on the Toarcian oceanic anoxic event in *Southiberian palaeomargin*. Sediment. Geol. 330, 59–73.
Guizhou Bureau of Geology and Minerals, 1987. Geological Marks of Guizhou Province. Geological Publishing House, Beijing, pp. 1–360 (in Chinese).
Hanilçi, N., 2013. Geological and geochemical evolution of the Bolkardaği bauxite deposits, Karaman, Turkey: transformation from shale to bauxite. J. Geochem. Explor. 133, 118–137.
Hou, B.H., Keeling, J., Li, Z., 2017. Paleovalley-related uranium deposits in Australia and China: a review of geological and exploration models and methods. Ore Geol. Rev. 88, 201–234.
Huang, Z.L., Jin, Z.G., Xiang, X.L., Gu, J., Wu, G.H., Chen, X.L., Su, Z.L., Zhao, Y.Y., Zuo, L., 2014. Mectallogenic Theory and Prediction of Bauxite Deposits in the Wuchunan-Zheng'an-Daozhen Area, Northern Guizhou Province. Science Press, China, pp. 89–99.
IAEA, 2009. World Distribution of Uranium Deposits (UDEPO) with Uranium Deposit Classification: IAEA-TECDOC-1629. 1179.
Jaireth, S., Roach, I.C., Bastrakov, E., Liu, S.F., 2015. Basin-related uranium mineral systems in Australia: a review of critical features. Ore Geol. Rev. 76, 360–394.
Kennedy, G.C., 1959. Phase relations in the system Al_2O_3-H_2O at high temperatures and

pressures. Am. J. Sci. 257 (10), 563–573.
Kittrick, J.A., 1969. Soil minerals in the Al_2O_3-SiO_2-H_2O system and a theory of their formation. Clay Clay Miner. 17, 157167.
Klauber, C., Gräfe, M., Power, G., 2009. Review of Bauxite Residue "Re-use" Options. CSIRO Document DMR-3609. National Research Flagships, Light Metals, Australia, pp. 1–79.
Klinkhammer, G.P., Palmer, M.R., 1991. Uranium in the oceans: where it goes and why. Geochim. Cosmochim. Acta 55, 1799–1806.
Kyser, K., Cuney, M., 2009. Unconformity-related uranium deposits. In: Cuney, M., Kyser, K. (Eds.), Recent and Not-so-recent Developments in Uranium Deposits and Implications for Exploration. Mineralogical Association of Canada and Society for Geology Applied to Mineral Deposits, Quebec, pp. 161–219.
Langmuir, D., 1978. Uranium solution-mineral equilibria at low temperatures with applications to sedimentary ore deposits. Geochim. Cosmochim. Acta 42(6, 547–569.
Li, J., Yu, B.S., Guo, F., 2013. Depositional setting and tectonic background analysis on Lower Cambrian black shales in the North of Guizhou Province. Acta Sedimentol. Sin. 31 (1), 20–31 (in Chinese with English abstract).
Li, Y.T., Xiao, J.F., Fu, S.H., Zhao, Z.J., 2014. The comparison study on metallogenic characteristics of the main bauxite-deposit-clustered areas in Guizhou province. Contrib. Geol. Min. Resour. Res. 4, 489–494 (in Chinese with English abstract).
Ling, K.Y., Zhu, X.Q., Tang, H.S., Wang, Z.G., et al., 2015. Mineralogical characteristics of the karstic bauxite deposits in the Xiuwen ore belt, Central Guizhou Province, Southwest China. Ore Geol. Rev. 65, 86–96.
Liu, P., 2001. Discussion on the metallogenic setting of the Qianzhong-Yu'nan bauxite in Guizhou and its genesi. Guizhou Gelogy 18 (4), 238–243 (In Chinese with English abstract).
Liu, P., Liao, Y.H., 2014. Regional metallogenic model and prospecting criteria of sedimentary bauxite deposits in Central Guizhou–Southern Chongqing region. Geol. China 41 (6), 2063–2082 (in Chinese with English abstract).
Liu, Z., Li, H., 2015. Metallurgical process for valuable elements recovery from red mud – a review. Hydrometallurgy 155 (Supplement C), 29–43.
Liu, Y., Naidu, R., 2014. Hidden values in bauxite residue (red mud): recovery of metals. Waste Manag. 34, 2662–2673.
Liu, X., Wang, Q., Zhang, Q., Yang, S., Liang, Y., Zhang, Y., Li, Y., Guan, T., 2017. Genesis of the Permian karstic Pingguo bauxite deposit, western Guangxi, China. Mineral. Deposita. http://dx.doi.org/10.1007/s00126-017-0723-y.
Long, Y.Z., Chi, G.X., Liu, J.P., Jin, Z.G., Dai, T.G., 2017. Trace and rare earth elements constraints on the sources of the Yunfeng paleo-karstic bauxite deposit in the Xiuwen-Qingzhen area, Guizhou, China. Ore Geol. Rev. 91, 404–418.
Lukas, T.C., Loughan, F.C., Eades, J.L., 1983. Origin of bauxite at Eufaula, Alabama, USA. Clay Miner. 18, 127–138.
Mei, M.X., Zhao, H., Meng, X.Q., Chen, Y.H., 2006. Sequence-stratigraphic framework and its forming background of palaeogeography for the middle Cambrian of the Upper-Yangtz region. Geol. J. China Univ. 12 (3), 328–342 (In Chinese with English abstract).
Mining 120, 2017. Distribution of Bauxite Ores in China. http://www.mining120.com/tech/show-htm-itemid-27919.html. Accessed December 2017.
Mo, B.H., Zhu, X.Y., Yao, Y.F., Sun, Z.X., Zhang, J., 2016. Analysis on uranium mineralization characteristics and ore-controlling factors of deposit 504, Guizhou. World Nuclear Geosci. 33 (1), 19–25 (in Chinese with English abstract).
Mongelli, G., 1997. Ce anomalies in the textural components of upper cretaceous karst bauxites from the Apulian carbonate platform (southern Italy). Chem. Geol. 140, 69–79.
Morse, J., Luther, G., 1999. Chemical influences on trace metal-sulfide interactions in anoxic sediments. Geochim. Cosmochim. Acta 63, 3373–3378.
Myllykylä, E., 2008. Reduction of Uranium in Disposal Conditions of Spent Nuclear Fuel, Working Report, Posiva. pp. 1–111.
Ni, S.J., Xu, Z.Q., Zhang, C.J., Song, H., Luo, C., 2012. Uranium metallogenesis and ore genesis of the rich-large black rock series-type uranium deposit in southwest China. Adv. Earth Science 27 (10), 1035–1041 (in Chinese with English abstract).
Palacios, M.L., Taylor, S.H., 2000. Characterization of uranium oxides using in-situ microRaman spectroscopy. Appl. Spectrosc. 54, 1372–1378.
Panahi, A., Young, G.M., Rainbird, R.H., 2000. Behavior of major and trace elements (including REE) during Paleoproterozoic pedogenesis and diagenetic alteration of an Archean granite near Ville Marie, Quebec, Canada. Geochim. Cosmochim. Acta 64, 2199–2220.
Pi, D.H., Liu, C.Q., Shields-Zhou, G.A., Jiang, S.Y., 2013. Trace and rare earth element geochemistry of black shale and kerogen in the early Cambrian Niutitang Formation in Guizhou province, South China: constraints for redox environments and origin of metal enrichments. Precambrian Res. 225, 218–229.
Pisarzowaka, A., Berner, Z.A., Racki, G., 2014. Geochemistry of Early Frasnian (Late Devonian) pyrite-ammonoid level in the Kostomłoty Basin, Poland, and a new proxy parameter for assessing the relative amount of syngenetic and diagenetic pyrite. Sediment. Geol. 308, 18–31.
Pitkänen, P., Partamies, S., Luukkonen, A., 2004. Hydrogeochemical Interpretation of Baseline Groundwater Conditions at the Olkiluoto Site. Posiva Report 2003–07, February 2004. Posiva Oy, Olkiluoto, Finland, pp. 159.
Pollack, G.D., Krogstad, E.J., Bekker, A., 2009. U–Th–Pb–REE systematics of organic-rich shales from the ca. 2.15 Ga Sengoma Argillite Formation, Botswana: evidence for oxidative continental weathering during the great oxidation event. Chem. Geol. 260, 172–185.
Richardson, K.A., 1959. The Thorium, Uranium and Zirconium Concentrations in Bauxites and their Relationship to Bauxite Genesis. 5. The rice institute, Houston, Texas, pp. 1–55.
Romberger, S.B., 1984. Transport and deposition of uranium in hydrothermal systems at temperatures up to 300 °C: Geological implications. In: Vivo, B.D., Capaldi, F.I.G., Simpson, P.R. (Eds.), Uranium Geochemistry, Mineralogy, Geology, Exploration and Resources. The Institution of Mining and Metallurgy, London, pp. 12–17.
Seredkin, M., Zabolotsky, A., Jeffress, G., 2016. In situ recovery, an alternative to conventional methods of mining: exploration, resource estimation, environmental issues, project evaluation and economics. Ore Geol. Rev. 79 (Supplement C), 500–514.
Skirrow, R.G., Jaireth, S., Huston, D.L., Bastrakov, E.N., Schofield, A., van der Wielen, S.E., Barnicoat, A.C., 2009. Uranium mineral systems, processes, exploration criteria and a new deposit framework. Geoscience Australia. Theatr. Rec. 44.
Smirnov, D.-I., Molchanova, T.-V., 1997. The investigation of sulphuric acid sorption recovery of scandium and uranium from the red mud of alumina production. Hydrometallurgy 45, 249–259.
Tang, Q.T., 2002. Enrichment factors of uranium at uranium deposit no. 138, Zhejiang Province. Uranium Deposit 18 (1), 41–45 (in Chinese with English abstract).
Tao, S., Tang, D., Zou, C., Li, J., Chen, X., Meng, C., 2009. Element geochemical characteristics of the lower assemblage hydrocarbon source rocks in Southeast Sichuan-Central Guizhou (Chuandongnan-Qianzhong) region and its periphery areas and their implications to sedimentary environments. Geol. China 36 (2), 397–403 (in Chinese with English abstract).
Taylor, S.R., McLennan, S.M., 1985. The Continental Crust: Its Composition and Evolution. Blackwell, Oxford, pp. 1–312.
Villar, L.P.d., Bruno, J., Campos, R., Gómez, P., Cózar, J.S., Garralón, A., Buil, B., Arcos, D., Carretero, G., Ruiz Sánchez-Porro, J., Hernán, P., 2002. The uranium ore from Mina Fe (Salamanca, Spain) as a natural analogue of processes in a spent fuel repository. Chem. Geol. 190, 395–415.
Wang, S., Zhang, J., 2016. Mineral and rock composition and resource properties of lower Cambrian black shale in Zhijin, Guizhou Province. Acta Petrol. Mineral. 3, 543–552 (in Chinese with English abstract).
Wang, Z.C., Zhou, X.M., Zhen, D.Y., Wang, G., Teng, R.Q., 2002. A metallogenetic model for Mesozoic unconformity-related uranium deposits in South China. Geol. Rev. 48 (4), 365–371 (in Chinese with English abstract).
Wang, Q., Liu, X., Yan, C., Cai, S., Li, Z., Wang, Y., Zhao, J., Li, G., 2012. Mineralogical and geochemical studies of boron-rich bauxite ore deposits in the Songqi region, SW Henan, China. Ore Geol. Rev. 48, 258–270.
Wilkin, R.T., Barnes, H.L., Brantley, S.L., 1996. The size distribution of framboidal pyrite in modern sediments: an indicator of redox conditions. Geochim. Cosmochim. Acta 60 (20), 3897–3912.
Wilkin, R.T., Arthur, M.A., Dean, W.E., 1997. History of water-column anoxia in the Black Sea indicated by pyrite framboid size distributions. Earth Planet. Sci. Lett. 148, 517–525.
Xiao, S.S., 1960. Radioactivity survey report in Lijiatian bauxite deposit, Luxi, Hunan. Geol. Prospect. Team Geol. Exploration Company of Hunan Metallurg. Bureau 173 (in Chinese, Unpublished).
Xiao, J.Q., Wang, Y., Zhong, J.R., Zhu, X.H., 2012. Raman spectroscopy and its application in analysis of uranium material. Chin. J. Spectrosc. Lab. 6, 3830–3835 (in Chinese with English abstract).
Yang, X.Y., Ling, M.X., Sun, W.D., Luo, X.D., Lai, X.D., Liu, Chi, Miao, J.Y., Sun, W., 2009. The genesis of sandstone-type uranium deposits in the Ordos Basin, NW China: constraints provided by fluid inclusions and stable isotopes. Int. Geol. Rev. 51 (5), 422–455.
Yang, E.L., Lu, X.B., Bao, M., Luo, J.J., Hu, Q.C., 2013. Enrichment and origin of some trace elements in black shales from the early Cambrian in eastern Guizhou Province. Adv. Earth Science 28 (10), 1160–1169.
Yao, Z.K., Zhen, D.Y., Liu, X., 1998. Metallogenic evolution of polygenetic and compound uranium ore deposits. Geol. Press 43–99 (in Chinese with English abstract).
Zhang, Z.W., Zhou, L.J., Li, Y.J., Wu, C.Q., Zheng, C.F., 2013. The "coal-bauxite-iron" structure in the ore-bearing rock series as a prospecting indicator for southeastern Guizhou bauxite mines. Ore Geol. Rev. 53, 145–158.
Zhang, L., Liu, C., Fayek, M., Wu, B., Lei, K., Cun, X., Sun, L., 2017. Hydrothermal mineralization in the sandstone–hosted Hangjinqi uranium deposit, North Ordos Basin, China. Ore Geol. Rev. 80, 103–115.
Zhao, F.M., 2009. An review on geology study of carbonaceous-siliceous-pelitic rock type uranium deposit in China and the strategy for its development. Uran. Geol. 25 (2), 91–97 (in Chinese with English abstract).
Zhao, K.D., Jiang, S.Y., Chen, W.F., Chen, P.R., Ling, H.F., 2014. Mineralogy, geochemistry and ore genesis of the Dawan uranium deposit in southern Hunan Province. J. Geochem. Explor. 138, 59–71.